Published in final edited form as:

Nature. 2019 July ; 571(7764): 279–283. doi:10.1038/s41586-019-1286-0.

Cryo-EM structure of oxysterol-bound human Smoothened coupled to a heterotrimeric G_i

Xiaofeng Qi[1,5], **Heng Liu**[2,5], **Bonne Thompson**[3], **Jeffrey McDonald**[1,3], **Cheng Zhang**[2,*], **Xiaochun Li**[1,4,*]

[1]Department of Molecular Genetics, University of Texas Southwestern Medical Center, Dallas, TX 75390;

[2]Department of Pharmacology and Chemical Biology, University of Pittsburgh, School of Medicine, Pittsburgh, PA15261;

[3]Center for Human Nutrition, University of Texas Southwestern Medical Center, Dallas, TX 75390

[4]Department of Biophysics, University of Texas Southwestern Medical Center, Dallas, TX 75390

Abstract

The oncoprotein Smoothened (SMO), a Frizzled-Class (Class-F) G-protein-coupled receptor (GPCR), transduces the Hedgehog (HH) signal from the tumor suppressor Patched-1 (PTCH1) to the glioma-associated oncogene (GLI) transcription factors, activating the signaling pathway[1,2]. It has remained a mystery how PTCH1 modulates SMO, how SMO is stimulated to form a complex with heterotrimeric G-proteins and whether G protein coupling contributes to GLI activation[3]. Here, we show that 24,25-epoxycholesterol (24,25-EC), identified as an endogenous ligand of PTCH1, can stimulate HH signaling in cells and trigger G protein signaling via human SMO (hSMO)*in vitro*. We further present a cryo-EM structure of 24(*S*),25-EC-bound hSMO coupledto a heterotrimeric G_i protein. The structure reveals a ligand binding site for 24(*S*),25-EC in the 7-transmembrane region (7-TMs) and a G_i-coupled activation mechanism of hSMO. Notably, the G_i protein presents a different arrangement from that of Class-A GPCR–G_i complexes. Therefore, our work provides molecular insights into HH signal transduction and the activation of a Class-F GPCR.

In the absence of HH, PTCH1 inhibits SMO[2]. This inhibition is thought to occur because PTCH1 may function indirectly by regulating a small molecule to modulate SMO[4]. Structural data suggest that HH binding may close a tunnel in PTCH1, allowing the putative sterol ligand to accumulate on the membrane for SMO activation[5–7]. SMO then activates GLI, causing transcription of HH target genes that promote cell proliferation and

*Correspondence should be addressed to C.Z. (chengzh@pitt.edu) or X.L. (xiaochun.li@utsouthwestern.edu).
[5]These authors contributed equally to this work.

Authors Contributions

X.Q. and X.L. conceived the project and designed the research with H.L and C.Z. B.T. and J.M. performed the sterol analysis by mass spectrometers. X.Q. purified the protein for mass spec analysis and H.L. purified the protein for cryo-EM study. X.Q. carried out cryo-EM work, built the model and refined the structure. X.Q. and H.L. performed the functional characterization. All the authors analyzed the data. X.Q., H.L., C.Z. and X.L. contributed to manuscript preparation. X.L. wrote the manuscript. Z.C. and X.L. supervised the project.

Competing interests The authors declare no competing financial interests.

differentiation[8]. The mechanism of how the signal transduces from PTCH1 to SMO remains elusive. It is known that the suppressor of fused (SUFU) represses GLI transcription factor activation, and active SMO releases this inhibition[9]. Previous studies showed that SMO activates G_i-family proteins, leading to a reduction of the intracellular concentration of cAMP[10,11], subsequently decreasing the activity of Protein Kinase A (PKA) and may either release the repression of PKA to GLI or engage other effectors.

Like other Class-F GPCRs, SMO has a cysteine-rich domain (CRD) at the amino terminus and 7-TMs. Previous structural studies revealed that the SMO-CRD can bind to sterol-like ligands to modulate the activity of SMO[12–14]. SMO contains a ligand-binding pocket in its 7-TMs that can bind agonistic or antagonistic ligands[12,15,16]. Class-F GPCRs play critical roles in the HH and Wnt pathways[17] and SMO is a drug target in the treatments of cancers[18]. Therefore, structural knowledge of Class-F GPCR activation is not only important for revealing the mechanism of HH and Wnt signal transduction, but also for developing potential therapeutic approaches.

Our previous structures showed three endogenous sterol-like densities in the extracellular domain I (ECD-I), Sterol-Sensing domain (SSD) and at the N-terminus of TM12 of the PTCH1 protein[5,6] (Fig.1a). Since PTCH1 may function as a sterol transporter, we speculated that the sterol-like density may be the agent responsible for transducing HH signal. The mass spectrometry analysis shows that the mixture of several oxysterols includes 24,25-EC, 24-keto-cholesterol (24k-C), 25-hydroxycholesterol (25-OHC), and 24-hydroxycholesterol (24-OHC) (Fig. 1b).

We added those oxysterols individually to SHH-light II cells that express SMO as well as a luciferase protein that is expressed from a GLI-dependent promoter. The results showed that 24(*S*)-OHC and 24(*S*),25-EC were more effective at activating HH signaling than other sterols at a concentration of 30 μM (Fig. 1c); in contrast, a previous study indicated that 100μM cholesterol was required to trigger HH signaling[13]. Remarkably, a recent study showed that 24,25-EC, the most abundant oxysterol in sea urchin embryo cilia, can activate HH signaling[19]. These findings suggest that 24(*S*),25-EC is one of the potential PTCH1 associated molecules that regulates SMO activity.

We further showed that 24(*S*),25-EC could stimulate G_i activation through SMO in GTPγS-binding assays as effectively as a synthetic SMO agonist, SAG, while cyclopamine lowered the GTPγS binding, acting as an inverse agonist (Fig. 1d). This observation is consistent with a previous study that demonstrated cyclopamine can bind the 7-TMs bundle of SMO mutants lacking the CRD (SMO-ΔCRD) to effectively suppress signaling[20,21]. HH signaling assay showed that the 24(*S*),25-EC-mediated stimulation of GLI activity was decreased by Pertussis toxin (PTX), an inhibitor of G_i, suggesting the involvement of G_i in HH signaling (Fig. 1e). Then, we assembled the SMO–G_i complex with 24(*S*),25-EC. A biochemical assay showed that the addition of GTPγS caused the dissociation of nucleotide-free complexes. Fab-G50, which binds to heterotrimeric G_i[22], was also added for the complex assembly (Extended Data Fig. 1).

The overall structure was determined at ~4 Å resolution (Extended Data Fig. 2). The density of hSMO-CRD was ambiguous, suggesting its high flexibility (Extended Data Fig. 2b and Methods). To improve the quality of cryo-EM map, we performed a masked classification of the complex with a subtraction of the signal from the CRD and the flexible region of Fab (Extended Data Fig. 2c). The resulting structure was determined to 3.9 Å resolution (Fig. 2a, Extended Data Figs. 2–4 and Table 1). The Fab-G50 fragment directly stabilizes the α-helical domain (AHD) of the $G\alpha_i$ and the Gβ subunits (Fig. 2a), similar to the structure of G_i-coupled rhodopsin[22]. Previous SMO structures indicated that the CRD binds oxysterols and cholesterol to activate SMO[12–14]. The cell biological data showed that SMO-ΔCRD has higher basal signaling activity than full-length SMO[21,23] suggesting that the CRD may stabilize SMO in a certain conformation, preventing excess signaling. These data along with our structural analysis imply that in our complex, SMO is in an active state and the CRD presents in a flexible conformation, allowing the recruitment of G proteins by 7-TMs.

A rod-shaped density was found in the 7-TMs (Extended Data Fig. 4c). Since 24(*S*),25-EC was added throughout the purification and previously reported structures of hSMO without 24(*S*),25-EC showed no density in this region[12] (Extended Data Fig. 5), we speculated that this density is 24(*S*),25-EC. It is consistent with studies that showed florescence-tagged oxysterols bind in the SMO-ΔCRD[19]. Structural analysis suggests that residue $N521^{7.41}$ may interact with the epoxy tail of 24(*S*),25-EC but is not involved in SAG binding (Fig. 2b and Extended Data Fig. 6a). The HH signaling assay showed that in the presence of 24(*S*),25-EC, the N521A mutant has a lower GLI-dependent HH signaling activity than the wild type; however, in the presence of SAG, this mutant and wild type showed a similar potency in triggering the signaling (Fig. 2c). The GTPγS binding assay showed that 24(*S*),25-EC can stimulate the binding of GTPgS to G_i by binding to SMO-ΔCRD and this effect can be reversed by cyclopamine (Fig. 2d), which has been shown to bind the 7-TMs of SMO[21,24] (Extended Data Fig. 6b). Such results suggest a binding-pocket for 24(*S*),25-EC in the 7-TMs of SMO. Then, we modeled 24(*S*),25-EC into the density. It is also possible that the CRD has a 24(*S*),25-EC binding site.

The ligand-binding pocket in the 7-TMs engages in the interaction with the antagonist Vismodegib[12], cyclopamine[14,24], LY2940680[15], SANT1[16] or the synthetic agonist SAG1.5[16] (Extended Data Fig. 6a–e). Interestingly, the different ligands occupy distinct positions in this pocket. Cyclopamine, LY2940680 and SAG1.5 are in the upper site of the pocket; in contrast, the Vismodegib and SANT1 and the putative 24(*S*),25-EC are in the lower site (Extended Data Fig. 6f).

The structure of G_i-coupled hSMO presents an active conformation with a predominant ~7Å outward movement of TM6 and a ~4Å movement of TM5 at the cytoplasmic surface as compared with the inactive hSMO (Fig. 3a). This is analogous to the structural changes upon activation of $G_{i/o}$-coupled Class-A GPCRs revealed by cryo-EM[22,25–28] Notably, structural comparison of G_i-coupled hSMO to inactive hSMO showed that not only the cytoplasmic end but also the entire TM6 move outward from the helical bundle (Extended Data Fig. 7a). Ligand binding introduces steric hindrance for residues $H470^{6.51}$ and $D473^{6.53}$, which move away from the ligand, leading to the outward movement and upper shift of the extracellular region of TM6 (Fig. 3b). This shift is linked to the larger outward movement of the

cytoplasmic portion of TM6 for G_i-coupling. Movement of residues F462$^{6.43}$ and V463$^{6.44}$ causes the shift of residues L412$^{5.55}$ in TM5 and T528$^{7.48}$ in TM7 (Fig. 3c). Their movement may be associated with the displacement of the cytoplasmic ends of TM5 and TM7 for G_i coupling.

Recently, the crystal structures of cholesterol-bound *Xenopus laevis* SMO (xSMO) and cyclopamine-bound xSMO have been reported[14]. It remains a mystery how xSMO presents in an active state while binding to cyclopamine, a natural antagonist[20].

Informative differences between the conformation of xSMO and G_i-coupled hSMO exist. First, the intracellular loops 2 and 3 (ICL2 and ICL3) of hSMO are clearly resolved dueto G_i-coupling (Fig. 3d); however, in the xSMO structure, the loops were either replaced for crystallization or were disordered. Second, R451$^{6.32}$ and W535$^{7.55}$ in the G_i-coupled hSMO still form a π-cation interaction unlike those in the xSMO (Fig. 3e). The distance between R451$^{6.32}$ and W535$^{7.55}$ in hSMO has changed from 4.5Å (inactive state) to 5Å (active state), suggesting a weakened but preserved π-cation interaction after G_i-coupling. There is an additional potential hydrogen bond between the side chain of R451$^{6.32}$ and the carbonyl group of T534$^{7.54}$. Therefore, the cytoplasmic ends of TM6 and TM7 may still interact after G_i-coupling. Residues R451$^{6.32}$ and W535$^{7.55}$ that are conserved in Class-F GPCRs were proposed to serve as a molecular switch in receptor activation[29]. Third, ICL-1 presents a shift in hSMO-G_i compared to xSMO; specifically, R261 changes its conformation to avoid clashing with $G\alpha_i$ (Fig. 3f). There is a tunnel through the middle of hSMO like xSMO (Fig. 3g). Since mutations located in the bottom of the tunnel abolish HH signaling[19], it is possible that another ligand can be transported through this tunnel to regulate SMO.

Class-A GPCRs have many conserved polar residues at the cytoplasmic region. These residues together with ions and water molecules mediate strong polar interactions to stabilize the 7-TMs in the inactive conformation[30]. However, there are very few polar residues in the cytoplasmic region of 7-TMs of hSMO (Extended Data Fig. 7b). Lack of polar interaction networks in SMO that stabilize the inactive conformation may result in a high receptor basal activity. It is tempting to speculate that such a structural feature may be associated with this high basal activity; therefore, a complex molecular machinery including PTCH1 is needed to negatively regulate SMO in cells. The agonist, which is still required to trigger the G protein signaling, may introduce a more efficient allosteric coupling to the cytoplasmic region, activating the receptor and allowing it to recruit G proteins.

The heterotrimeric G_i has been modeled from the density map (Extended Data Fig. 4). The major contact between hSMO and $G\alpha_i$ is created by ICLs 1–3, TM3 and TMs 5–7 of hSMO and the αN, αN–β1 loop and α5-helix of the $G\alpha_i$ (Fig. 4a). The C-terminus of the α5-helix of $G\alpha_i$ inserts into the intracellular groove of hSMO (Fig. 4a). The residues in ICL3, TM5 and TM6 engage in the interactions with the α5-helix of the $G\alpha_i$. ICL2 and the C-terminus of TM3 also cooperate with the α5-helix in addition to touching the C-terminal residues of αN of $G\alpha_i$. Moreover, R257 in ICL1 has a hydrophilic interaction with D312 of Gβ, stabilizing the complex (Fig. 4b).

After binding hSMO, the α5-helix of $G\alpha_i$ undergoes a conformational change with a translation of more than 5Å and a ~90° rotation (Fig. 4c). The movement of the α5-helix induces a shift of the β6–α5 loop of more than 5Å triggering the dissociation of GDP (Fig. 4d). Furthermore, the AHD moves away from the Ras-like domain to bind the Gβ subunit and Fab-G50 as in the structure of rhodopsin-G_i (Fig. 4e). The similarities between G_i coupling to SMO with Class-A GPCRs reveal that the mechanism of G_i activation by SMO is shared with Class-A GPCRs[22,25–27](Extended Data Fig. 8). Superposing the structure of hSMO with G_i-coupled μOR shows a different orientation of the G_i protein relative to the receptor (Fig. 5a). Superposing the receptors from hSMO-G_i and the other four G_i-coupled complexes reveals that the ICL2 and ICL3 of hSMO face inward towards the α5-helix of $G\alpha_i$ (Fig. 5b). Consistently, the α5-helix is the major contact site with the receptor. Interestingly, it is parallel to the 7-TMs of hSMO (Fig. 2a) with a ~4–5Å tilt compared to that of the G_i-coupled Class-A GPCRs (Fig. 5c).

Comparison with the μOR-G_i complex reveals that the different arrangements of the α5-helix of $G\alpha_i$ with respect to the receptors cause the $G\alpha_i$-αN to rotate by 30° (Fig. 5d) and the Gβ and Gγ of hSMO-G_i complex to move 20Å away from the receptor (Fig. 5d). Comparison with the G_i protein in the rhodopsin-G_i complex shows that the $G\alpha_i$-αN is rotated by about 10° and the shift of α5-helix of $G\alpha_i$ introduced a 20Å movement of $G\alpha_i$-AHD (Fig. 5e). As a result, the outward displacement of TM6 is less prominent compared with the TM6 of Class-A GPCRs for G_i coupling (Fig. 5b). Such pronounced structural differences attest to a high degree the versatility of G_i for coupling to receptors. Indeed, it has been suggested that more GPCRs couple to $G_{i/o}$ proteins than to other G protein families[25]. Recently, the structure of hFZD4, another Class-F GPCR, was reported[31]. The apo hFZD4 shares a similar conformation as the inactive hSMO (Extended Data Fig. 9). It requires further investigations on whether FZDs couple to G-proteins in the same way as SMO.

Other studies indicated that other oxysterols and/or cholesterol can also stimulate HH signal through SMO[13,19,21,32]. Specifically, they showed that the inhibition of oxysterol or cholesterol synthase can block HH signal in cells and the signaling can be rescued by the addition of different oxysterols[19,32]. It is possible that either cholesterol or oxysterols can be associated with SMO as endogenous ligands to regulate the signal. Here, we used 24(*S*),25-EC as a prototype to reveal how oxysterol can stimulate HH signaling and trigger SMO activation for G protein signaling. Our structure reveals a novel pattern of GPCR-G_i coupling (Fig. 5). Besides G_i protein, β-arrestins also have been shown to regulate SMO localization and signaling[33]. Structures of β-arrestin–SMO complexes may be a future research focus.

Methods

Identification of oxysterols from PTCH1

Human Patched-1 with the C-terminal domain and internal loop truncation (PTCH1*) was expressed and purified as described before[5,6]. The Flag-tagged protein was purified in digitonin using gel filtration. To avoid exogenous contamination, we did not introduce any lipids or sterol derivatives during the purification. The small, nonpolar molecules were

extracted using a liquid-liquid extraction of dichloromethane, methanol, and aqueous buffer (20 mM Hepes pH7.5, 150 mM NaCl and 0.06% digitonin) in 1:1:1 ratio. The mixture was vortexed, centrifuged and the organic phase removed to a fresh tube. This extraction was repeated by adding an additional volume of dichloromethane to the aqueous fraction, vortexing, centrifuging, and pooling the organic extract with the first. The lipid extract was dried under N_2 gas with gentle heat (~45°C) to evaporate the organic solvent. Dried samples were dissolved in 90% methanol and subject to LCMS as described[34]. Results are shown as mean ± s.d. from 3 biologically independent experiments.

Protein expression and purification

Human Smoothened (hSMO) with a C-terminal truncation (Δ556–787) was cloned into pEG BacMam with a C-terminal Flag tag. The protein was expressed using baculovirus-mediated transduction of mammalian HEK-293S GnTI$^-$ cells (ATCC). 1L of cell culture was pelleted by centrifugation and resuspended in 20 ml buffer containing 20 mM HEPES pH 7.5, 150 mM NaCl, 0.2 μg/ml leupeptin, 150 μg/ml benzamidine and 1μM 24(*S*),25-EC (Abcam). After 30 min incubation at 25 °C, 20 ml 2X solubilization buffer containing 20 mM HEPES pH 7.5, 150 mM NaCl, 1% dodecyl-maltoside (DDM), 0.2% cholesterol hemisuccinate (CHS), 20% glycerol, 0.2 μg/ml leupeptin, 150 μg/ml benzamidine, 1μM 24(*S*),25-EC and 5 U Salt Active Nuclease (Sigma) was added. Cell membranes were disrupted by repeated Dounce homogenization and solubilized for 1 hour at 4 °C. The supernatant was collected by centrifugation at 25,000 g for 30 min at 4 °C, and then incubated with anti-Flag M2 antibody resin for 1 hour at 4°C. After washing three times in batch with buffer containing 20 mM HEPES pH 7.5, 150 mM NaCl, 0.1% DDM, 0.02% CHS, 0.2 μg/ml leupeptin, 150 μg/ml benzamidine, and 1μM 24(*S*),25-EC, the resin was transferred to a gravity column. After extensive washing, the receptor was eluted from M2 resin using the buffer containing 20 mM HEPES pH 7.5, 100 mM NaCl, 0.1% DDM, 0.02% CHS, 200μg/ml Flag peptide (GL Biochem) and 1μM 24(*S*),25-EC.

Constructs, expression and purification of G_i heterotrimer

G protein expression and purification was performed based on a published method[35]. In general, the wild type $G\alpha_i1$ and a dominant-negative human $G\alpha_i1$ mutant (S47N, G204A, E246A and A327S) were cloned into a pFastbac vector without any tag, and the virus was prepared using the Bac-to-Bac system (Invitrogen). N-terminal 6×His-tagged human Gβ1, and human Gγ2 were cloned into pVL1392 vector, and the virus was prepared using the BestBac system (Expression Systems, LLC). The heterotrimeirc G_i complex was expressed in Sf9 insect cells (Invitrogen). The cells at a cell density of 4×10^6 per ml were infected with both $G\alpha_i$ and Gβγ virus at a ratio of 10:1 per liter at 27 °C for 48 hours before harvesting. Cells were harvested by centrifugation and lysed in lysis buffer (10 mM Tris, pH 7.5, 100 μM $MgCl_2$, 5 mM β-mercaptoethanol (β-ME), 10 μM GDP, 0.2 μg/ml leupeptin and 150 μg/ml benzamidine). The cell membrane was collected by centrifugation at 25,000 g for 30 min at 4 °C. Cell membranes were disrupted by repeated Dounce homogenization and solubilized in solubilization buffer (20mM HEPES pH 7.5, 100 mM NaCl, 1% sodium cholate, 0.05% DDM, 5 mM $MgCl_2$, 2 μL CIP, 5mM β-ME, 10 μM GDP, 10% glycerol, 0.2 μg/ml leupeptin and 150 μg/ml benzamidine). The supernatant was separated by centrifugation at 25,000 g for 30 min, and incubated with Ni-NTA agarose resin (Clontech)

in batch for 1 hour at 4 °C. The resin was then washed in batch with solubilization buffer and transferred to a gravity column. The buffer was exchanged on column from solubilization buffer to wash buffer comprised of 20 mM HEPES pH 7.5, 50 mM NaCl, 0.1% DDM, 1 mM $MgCl_2$, 5 mM β-ME, 10 μM GDP, 0.2 μg/ml leupeptin and 150 μg/ml benzamidine. The protein was eluted in wash buffer with 250 mM Imidazole, and treated with Lambda Phosphatase (New England BioLabs) and Alkaline Phosphatase (New England BioLabs) overnight at 4 °C. The protein was further purified with anion exchange chromatography. The low salt buffer is comprised of 20 mM HEPES pH 7.5, 40 mM NaCl, 0.1% DDM, 1 mM $MgCl_2$, 100 μM TCEP, 10 μM GDP. The high salt buffer was prepared as low salt buffer but with 1M NaCl. The pure protein was supplemented with 10% glycerol, concentrated to ~20mg/ml, flash-frozen in liquid nitrogen, and stored at −80 °C.

Assembly of hSMO-G_i-Fab complex

Purified hSMO was mixed with the dominant-negative G_i heterotrimer at a 1:1.3 molar ratio. This mixture was incubated at 25°C for 1 hour followed by addition of apyrase to catalyze the hydrolysis of unbound GDP to stabilize the nucleotide-free complex overnight at 4°C. To remove excess G_i protein, the mixture was purified by anti-Flag M2 antibody affinity chromatography. Detergent was exchanged from 0.1% DDM to 0.01% lauryl maltose neopentyl glycol (MNG) on the M2 resin. The complex was eluted using the buffer comprised of 20 mM HEPES pH 7.5, 100 mM NaCl, 0.01% MNG, 0.001% CHS, 1μM 24(*S*),25-EC, 200 μg/ml Flag peptide. Finally, a 1.3 molar excess of Fab-G50 prepared as previously reported[22] was added to the elution. The hSMO–G_i–Fab complex was purified and buffer-exchanged by size exclusion chromatography with buffer containing 20 mM HEPES pH 7.5, 100 mM NaCl, 0.002% MNG, 0.001% CHS, 0.001% GDN, 0.002% digitonin and 1μM 24(*S*),25-EC. Peak fractions were concentrated to ~ 5–10 mg/ml for electron microscopy studies.

EM Sample Preparation and Imaging

The freshly purified hSMO–G_i–Fab complex was added to Quantifoil R1.2/1.3 400 mesh Au holey carbon grids (Quantifoil), blotted using a Vitrobot Mark IV (FEI), and frozen in liquid ethane. The grids were imaged in a 300 keV Titan Krios (FEI) with a Gatan K2 Summit direct electron detector (Gatan). Data were collected in super-resolution mode at a pixel size of 0.535 Å with a dose rate of 2 electrons per pixel per second. Images were recorded for 10 s exposures in 50 subframes to give a total dose of 70 electrons per $Å^2$.

Imaging Processing and 3D reconstruction

Dark subtracted images were normalized by gain reference and binned 2 fold that resulted in the original pixel size of 1.07 Å. Drift correction was performed using the program MotionCor2[36]. The contrast transfer function (CTF) was estimated using CTFFIND4[37]. To generate hSMO–G_i–Fab complex templates for automatic picking, around 2000 particles were manually picked and classified by 2D classification in RELION[38]. After auto-picking in RELION, the low-quality images and false-positive particles were removed manually. About 469k particles were extracted for subsequent 2D and 3D classification.

We used the cryo-EM structure of G_o–5-$HT_{1B}R$ complex (EMD-4358) at low-passfiltered to 60 Å as the initial model for 3D classification in RELION. The model of best class after 3D classification was used as the initial model for the final 3D classificationand 3D auto-refinement in RELION. To identify the position of the CRD in the cryo-EM map, we classified the particles using a CRD mask, refined the structure with a CRDmask or performed multibody refinement; however, the map of CRD remained very weak. Therefore, we conclude that the CRD of SMO adopts a flexible conformation in the active state.

The final refinement was performed in FREALIGN[39] using this best class as the initial model. The global search was performed once without mask followed by another global search using the mask, which was generated using "relion_mask_create" excluding the micelle. The full map is estimated to be 4 Å using the 0.143 cutoff criteria. For the truncated map, about 330k particles selected from 2D classification were subtracted by RELION to remove the signal of the CRD and half of the Fab (the dash circles in Extended Data Fig. 2b). 3D classification, 3D auto-refinement and unmasked refinement in FREALIGN were performed as the full map. 141,100 particles were selected for 3D auto-refinement and FREALIGN refinement. A CRD and half of the Fab truncated mask with 6 Å extensions was used for the masked refinement in FREALIGN, with a BSC value of 10 to further exclude the bad particles. The final subtracted map without the CRD and half of the Fab is estimated to be 3.84 Å using the 0.143 cutoff criteria.

Model Construction

The subtracted map was used for the model building and refinement. To obtain better side-chain densities for model building, we sharpened the map using BFACTOR.EXE (author: Nikolaus Grigorieff) with a resolution limit of 3.9 Å and a B-factor value of −100 $Å^2$. The structure of human SMO (PDB: 5L7D) with the CRD deletion and the structure of $G\alpha_i1\beta1\gamma2$ and Fab-G50 from the rhodopsin–G_i–Fab complex (PDB: 6CMO) were docked to the map as the initial model. The structure model was manually built by COOT[40]. The residues 1–189 (CRD) and 554–787 (C-terminus) of hSMO were not built. Half of the Fab-G50 (5–108 of the light chain and 5–130 of the heavy chain) was built.

Model Refinement and Validation

The model was refined in real space using PHENIX[41] and also in reciprocal space using Refmac with secondary-structure restraints and stereochemical restraints[42,43]. Structure factors were calculated from a half-map (working) using the program SFall[44]. Fourier shell correlations (FSCs) were calculated between the two half maps, the model against the working map, the other (free) half map, and full (sum) map[45]. Local resolutions were estimated using Blocres[46]. MolProbity[47] was used to validate the geometries of the model. Structure figures were generated using PyMOL (http://www.pymol.org) and Chimera[48].

^{35}S-GTPγS Binding Assay

The membrane of HEK293 cells overexpressing hSMO (~200 μg/ml) or hSMO-ΔCRD (with the residues 1–189 deleted) with a C-terminal flag tag was incubated with 200 nM purified G_i protein for 30 minutes on ice in buffer containing 20 mM HEPES pH 7.5, 100 mM NaCl, 5mM $MgCl_2$, 3 μg/ml BSA, 0.1μM TCEP, and 5μM GDP to get the receptor and G_i

complex. Next, 25 μL aliquots of the pre-formed complex were mixed with 225 μL reaction buffer containing 20 mM HEPES, pH 7.5, 100 mM NaCl, 5mM $MgCl_2$, 3 μg/ml BSA, 0.1μM TCEP, 1μM GDP, 35 pM ^{35}S-GTPγS (Perkin Elmer) and ligands. For Fig. 1d, 50 μM of cyclopamine (Cayman Chemical), SAG (Tocris Bioscience) or 24(*S*),25-EC were used. For the competition assays in Fig. 2d, 10 μM cyclopamine, 10 μM 24(*S*),25-EC and 10 μM 24(*S*),25-EC plus 100 μM cyclopamine were used. After additional 10 min incubation at 25 °C, the reaction was terminated by adding 4 ml of cold wash buffer containing 20 mM HEPES pH 7.5, 100 mM NaCl and 5mM $MgCl_2$, and filtering through glass giber prefilters (Millipore Sigma). After washing three times with 4 ml cold wash buffer, the filters were incubated with 5 ml of CytoScint liquid scintillation cocktail (MP Biomedicals) and counted on a Beckman LS6500 scintillation counter to determine the binding of ^{35}S-GTPγS to G_i induced by hSMO activation. The data analysis was performed using GraphPad Prism 7 (GraphPad Software). Results are shown as mean ± s.d. from 3 biologically independent experiments.

HH Reporter Assays

The SHH-N conditioned medium was obtained as described before[5,6]. All the sterols were solubilized in 10-fold (molar ratio) methylated β-cyclodextrin (MCD, from Trappsol). SHH Light II cells, a stable cell line expressing firefly luciferase with an 8XGli promoter and Renilla luciferase with a constitutive promoter, were used to measure HH pathway activity. SHH Light II cells were treated with the conditioned medium, sterols and pertussis toxin (PTX, from Invitrogen) for 30 hours before measuring. To detect the activity of SMO variants in HH signaling, the 8X-Gli-Firefly luciferase reporter transgene, a constitutive Renilla luciferase transgene, and a pcDNA3.1 vector encoding wild-type hSMO or N521A mutant were transfected to *Smo*$^{-/-}$ MEFs using TransIT reagent (Mirus Bio LLC). After 24 hours, cells were serum-starved in DMEM with 0.5% FBS. 24 hours later, cells were treated with 30 μM 24(*S*),25-EC or 100 nM SAG for another 24 hours. Firefly and Renilla luciferase activity were measured using the Dual-Luciferase® Reporter Assay System (Promega). The data analysis was performed using GraphPad Prism 7 (GraphPad Software). Results are shown as mean ± s.d. from 3 biologically independent experiments.

Data and Materials Availability: The data that support the findings of this study are available from the corresponding author upon request. The 3D cryo-EM density map has been deposited in the Electron Microscopy Data Bank under the accession number EMD-20190. Atomic coordinates for the atomic model have been deposited in the Protein Data Bank under the accession number 6OT0.

Extended Data

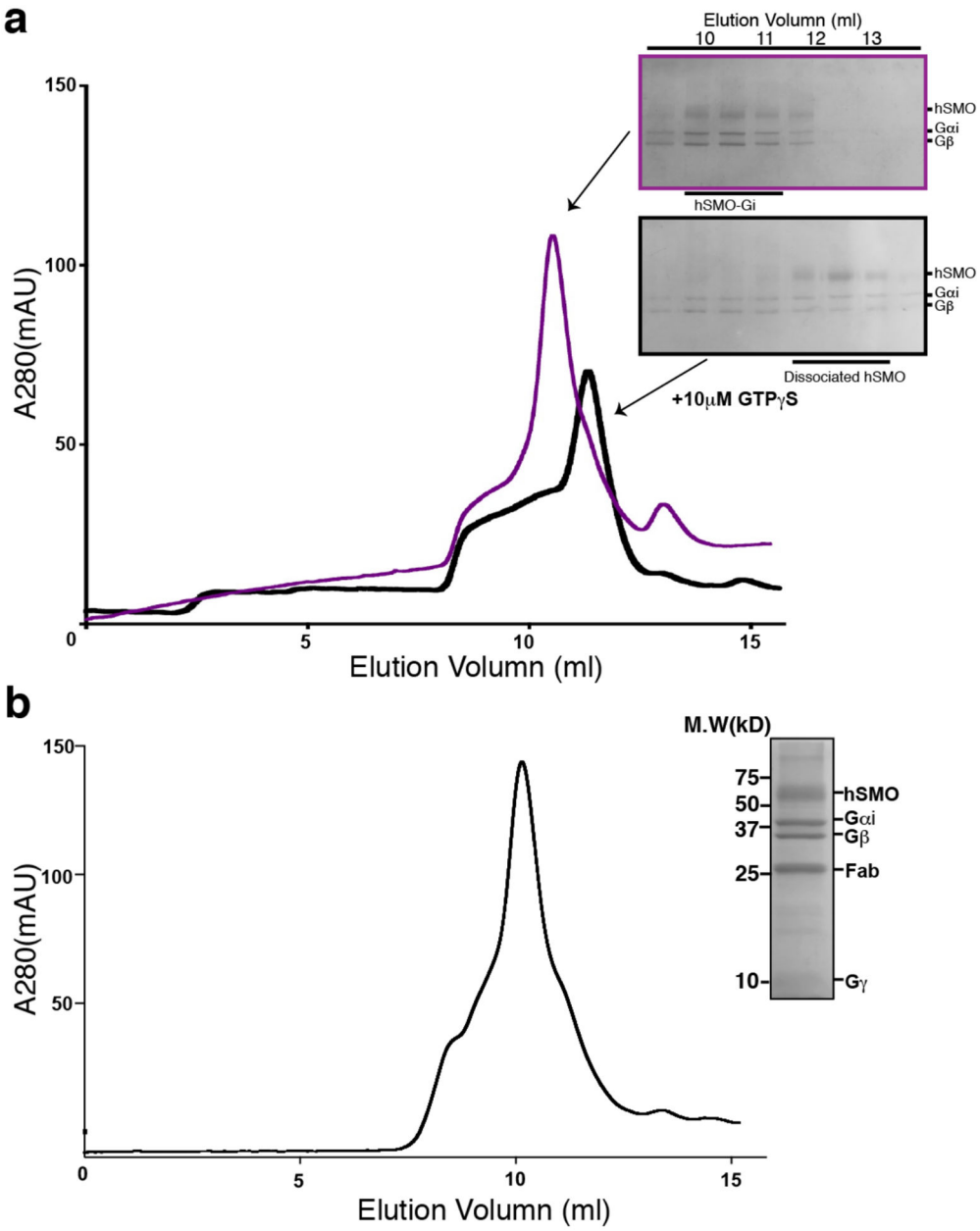

Extended Data Fig. 1. Assembly of hSMO–G_i–Fab complex

a, GTPγS causes the dissociation of 24(*S*),25-EC mediated hSMO–G_i complex. **b**, Size-exclusion chromatogram and SDS–PAGE gel of the purified hSMO–G_i–Fab complex. Molecular standards are indicated on left side of the gel.

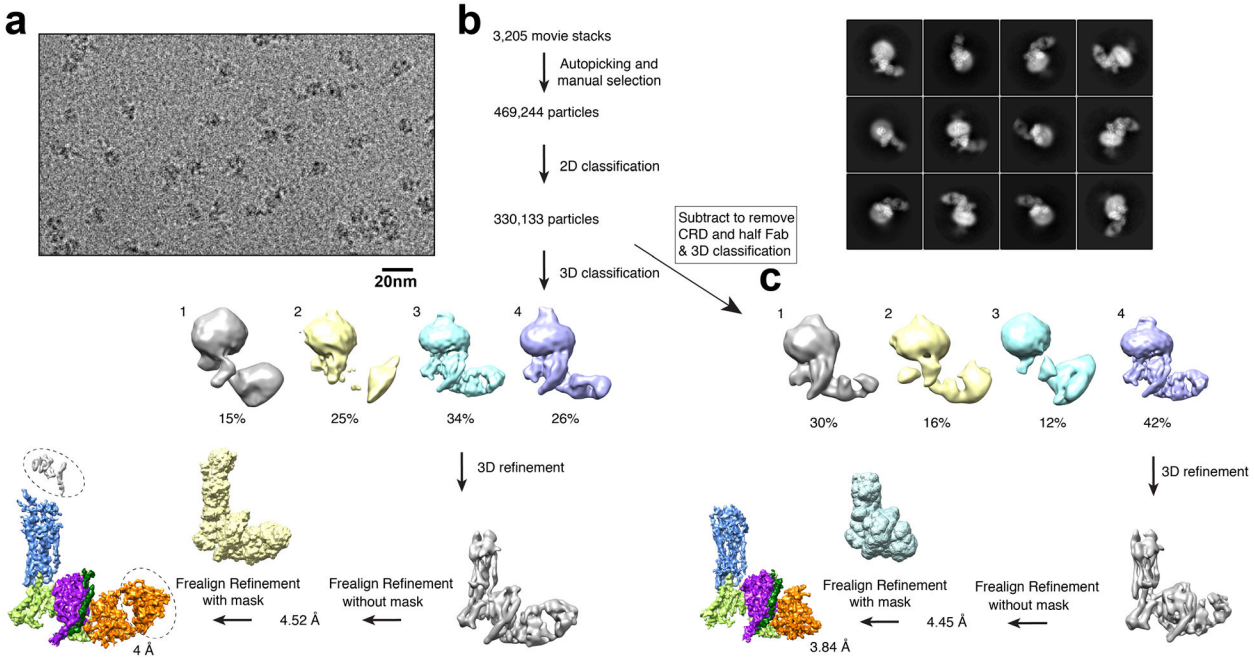

Extended Data Fig. 2. Data processing.

a, A representative electron micrograph at −2.0 μm defocus. **b**, The data processing workflow for the complex with the full map. The cryo-EM 2D classification from RELION is shown. The subtracted parts were indicated by dash circles. **c**, The data processing workflow for the complex with the subtracted map. Class 3 of the full map and Class 4 of the subtracted map were used for the final refinement; Class 4 of the full map and Class 1 of the subtracted map failed to have sufficient structural features in the final refinement. Masks used for the refinement are shown. The cryo-EM map after Frealign refinement sharpened using BFACTOR.EXE (author: Nikolaus Grigorieff) with a resolution limit of 4 Å or 3.9 Å and a B-factor value of −100 $Å^2$. Each subunit is colored.

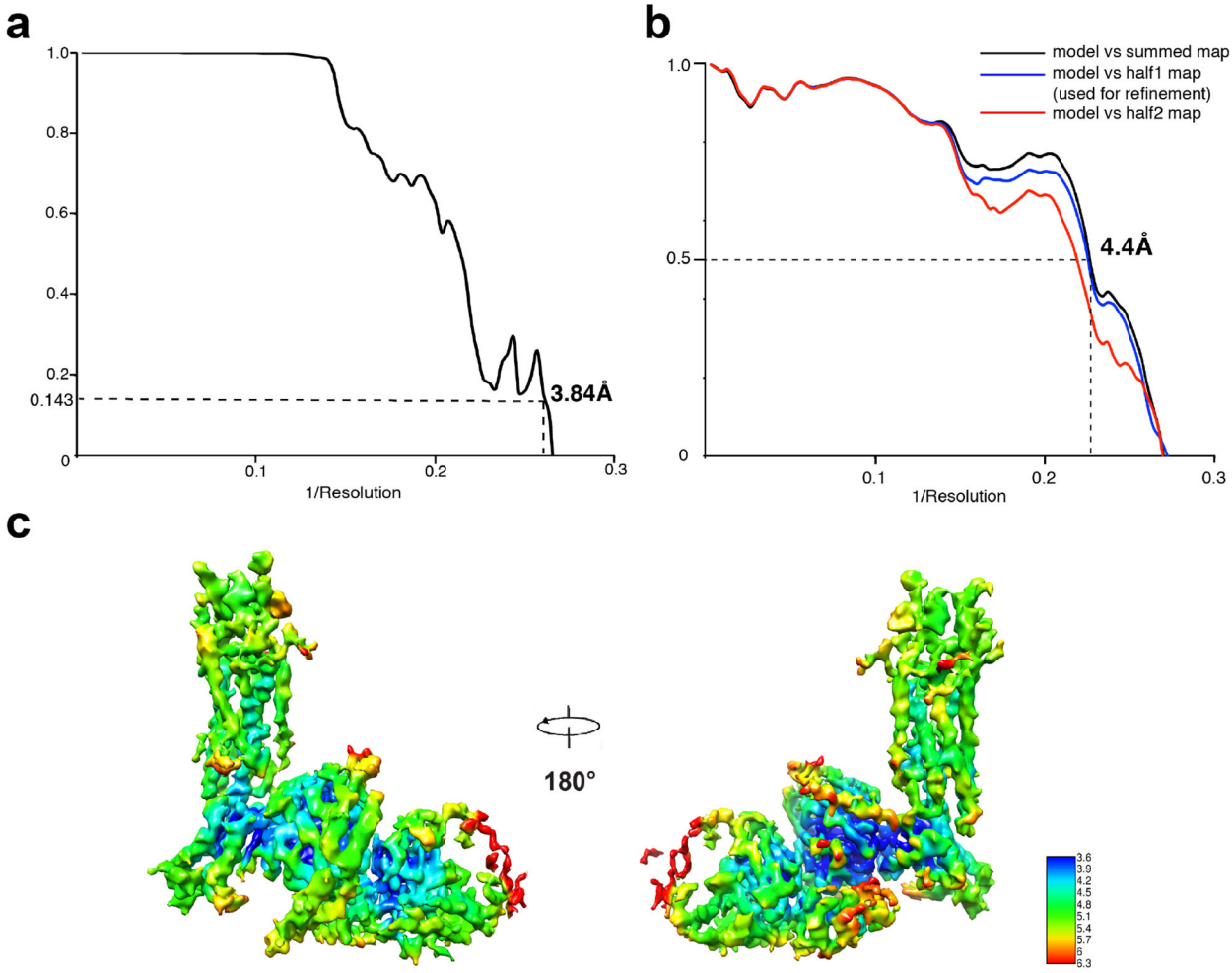

Extended Data Fig. 3. The model quality assessment.

a, Fourier shell correlation (FSC) curve of the structure without the CRD and half Fab with FSC as a function of resolution using Frealign output. **b**, The FSC curves calculated between the refined structure and the half map used for refinement (blue), the other half map (red) and the full map (black). **c**, Density maps of structure colored by local resolution estimation using Blocres.

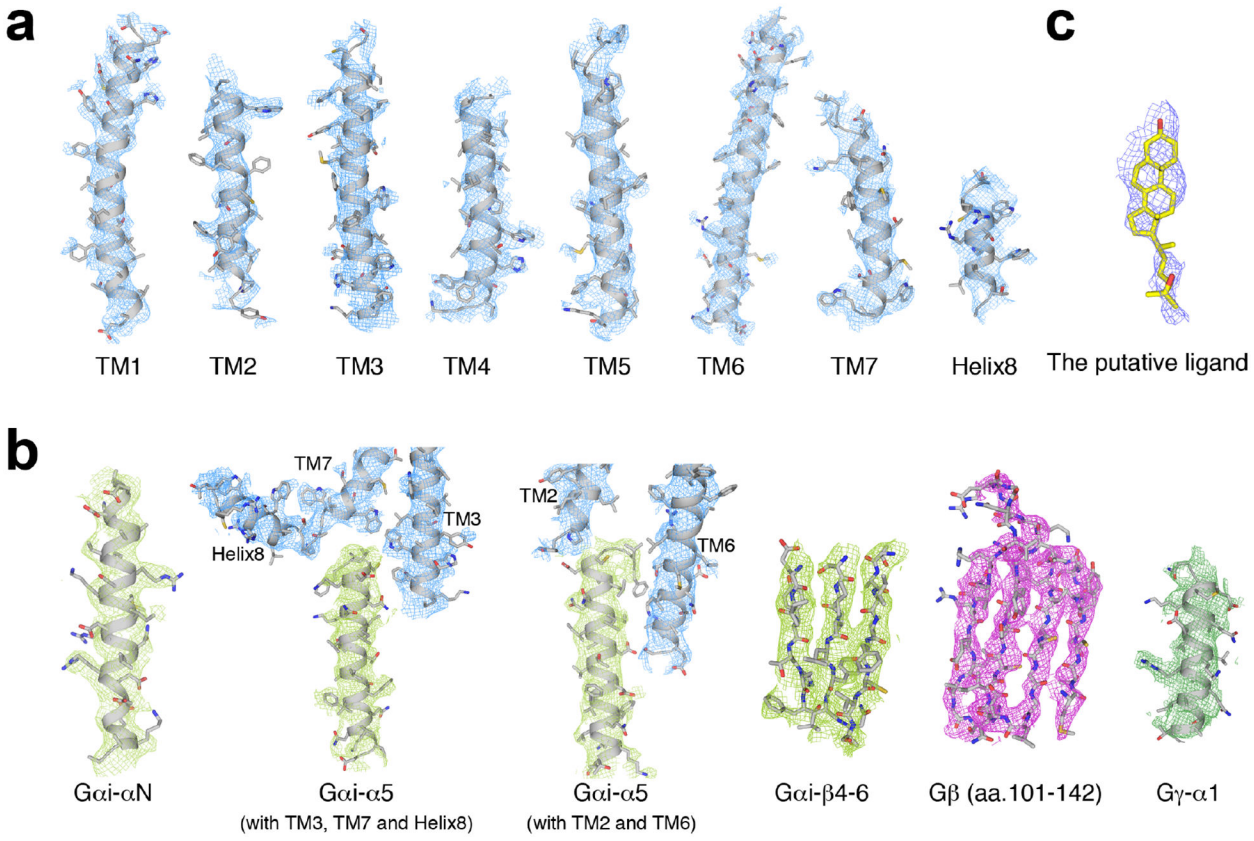

Extended Data Fig. 4. cryo-EM map of structural elements in the complex.

a, The major helices of hSMO. **b**, The major structural elements of G_i protein. EM density map and model of the complex are shown in mesh and cartoon. **c**, the putative ligand.

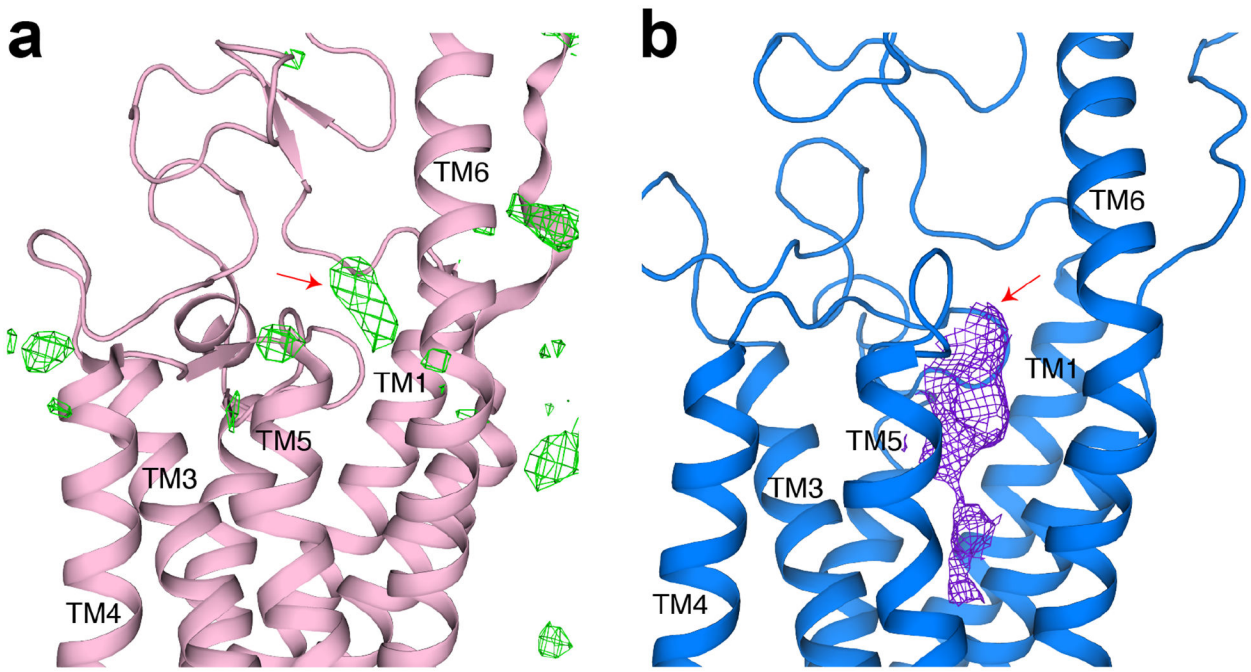

Extended Data Fig. 5. Comparison of the maps in the ligand-binding pocket of hSMO.

a, The extra density within the TMD ligand-binding pocket in the hSMO crystal structure (PDB: 5L7D). The density is shown in green at 3σ level and indicated by arrow. **b**, The density of the ligand in the G_i–hSMO complex. The density is shown in purple mesh at 5σ level at 3.9Å and indicated by arrow.

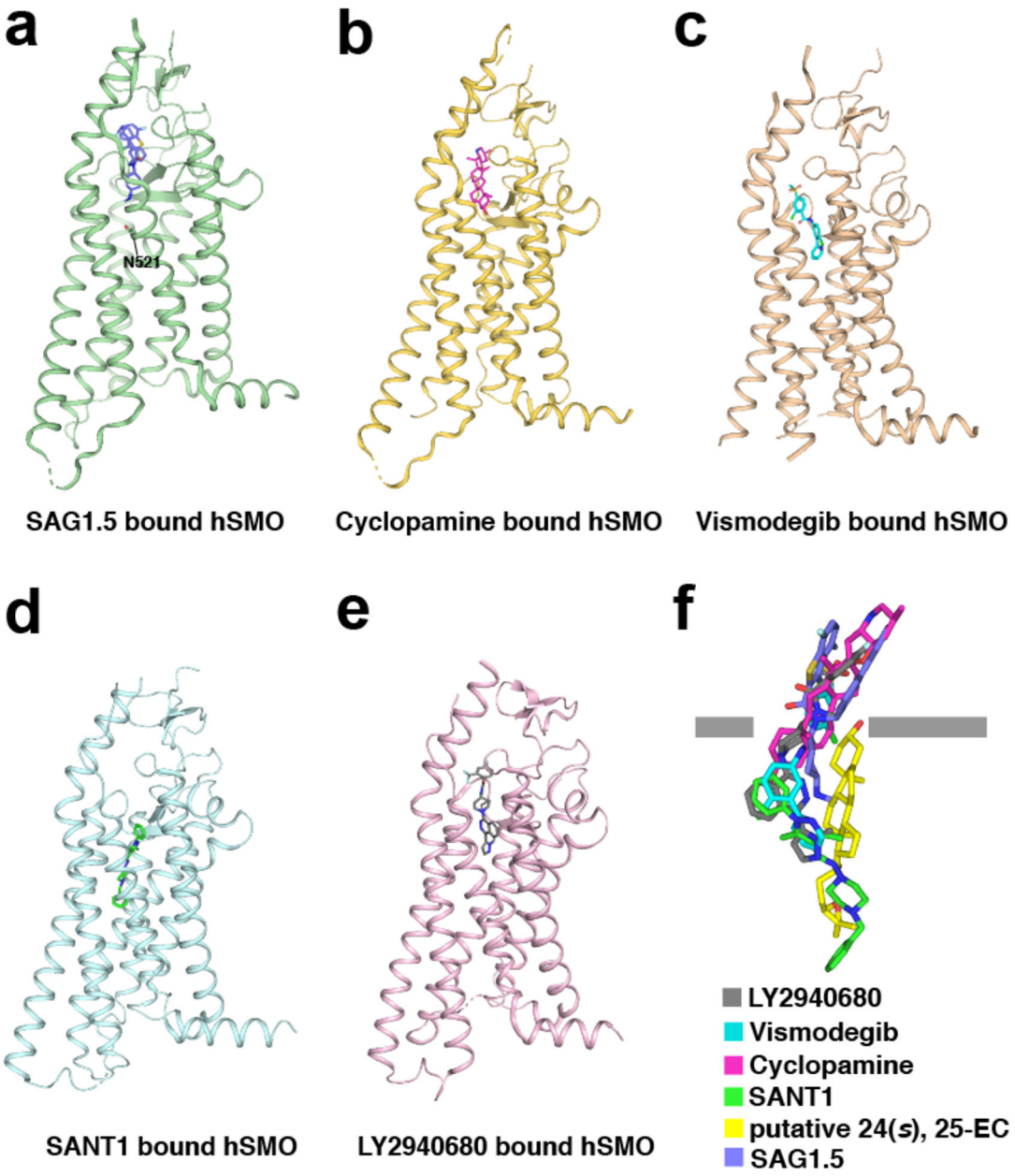

Extended Data Fig. 6. Comparison of the binding sites of different SMO ligands.

a, SAG1.5 bound hSMO (PDB:4QIN)**. b**, Cyclopamine bound hSMO (PDB: 4O9R). **c**, Vismodegib bound hSMO (PDB: 5L7I). **d**, SANT1 bound hSMO (PDB:4N4W). **e**, LY2940680 bound hSMO (PDB:4JKV). Structures of hSMO with different ligands viewed from the side of the membrane. **f**, Superimposition of the ligands that bind the pocket in the transmembrane domain of hSMO.

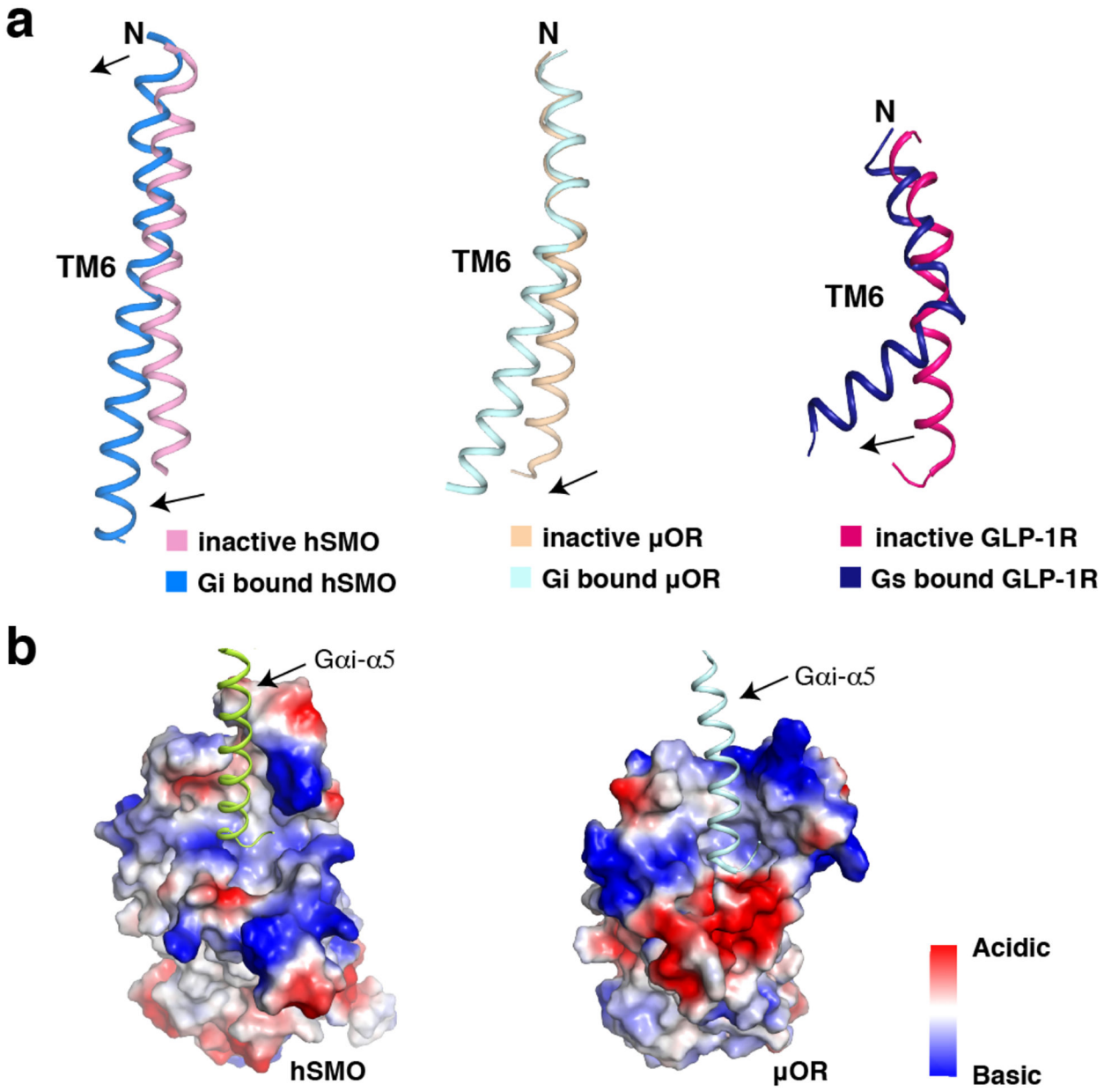

Extended Data Fig. 7. Comparisons of the TM6s and cytosolic sites of hSMO and μOR.

a, Structural comparison of TM6s of hSMO, μOR and GLP-1R in the inactive and G protein-bound states. Left: hSMO, inactive SMO in pink (PDB: 5L7D); Middle: μOR, inactive μOR in light orange (PDB: 4DKL), G_i-μOR in light cyan (PDB: 6DDE); Right: GLP-1R, inactive GLP-1R in red (PDB: 5VEW), G_s-GLP-1R (PDB: 6B3J) in dark blue. **b**, Electrostatic surface representations of the cytosolic side of SMO and μOR complex with $G\alpha_i$-α5.

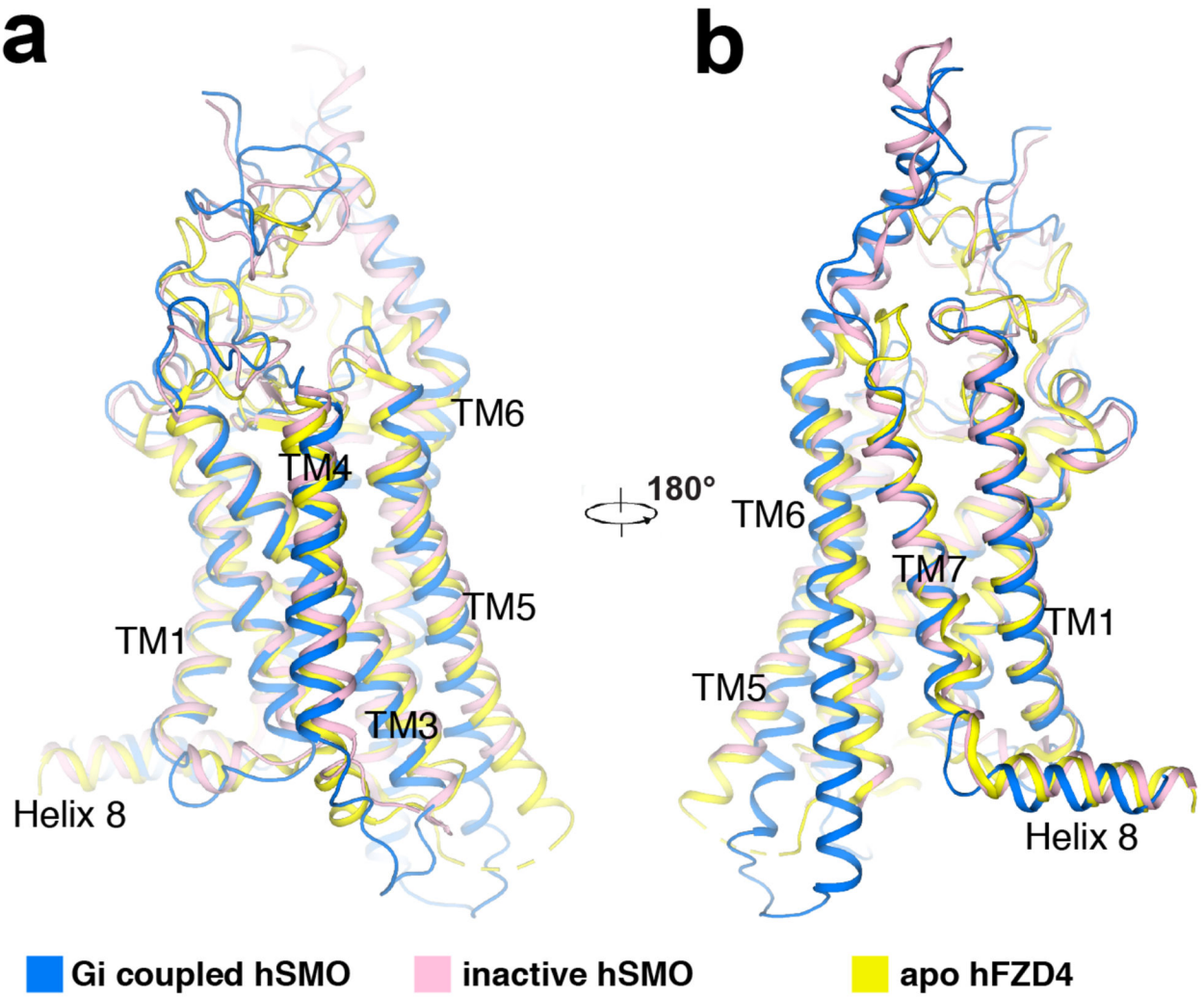

Extended Data Fig. 8. The structures of G_i-bound Class-A GPCRs.

a, Rhodopsin-G_i complex (PDB: 6CMO). **b**, A_1R-G_i complex (PDB: 6D9H). **c**, μOR-G_i complex (PDB: 6DDE). **d**, CB1-G_i complex (PDB: 6N4B).

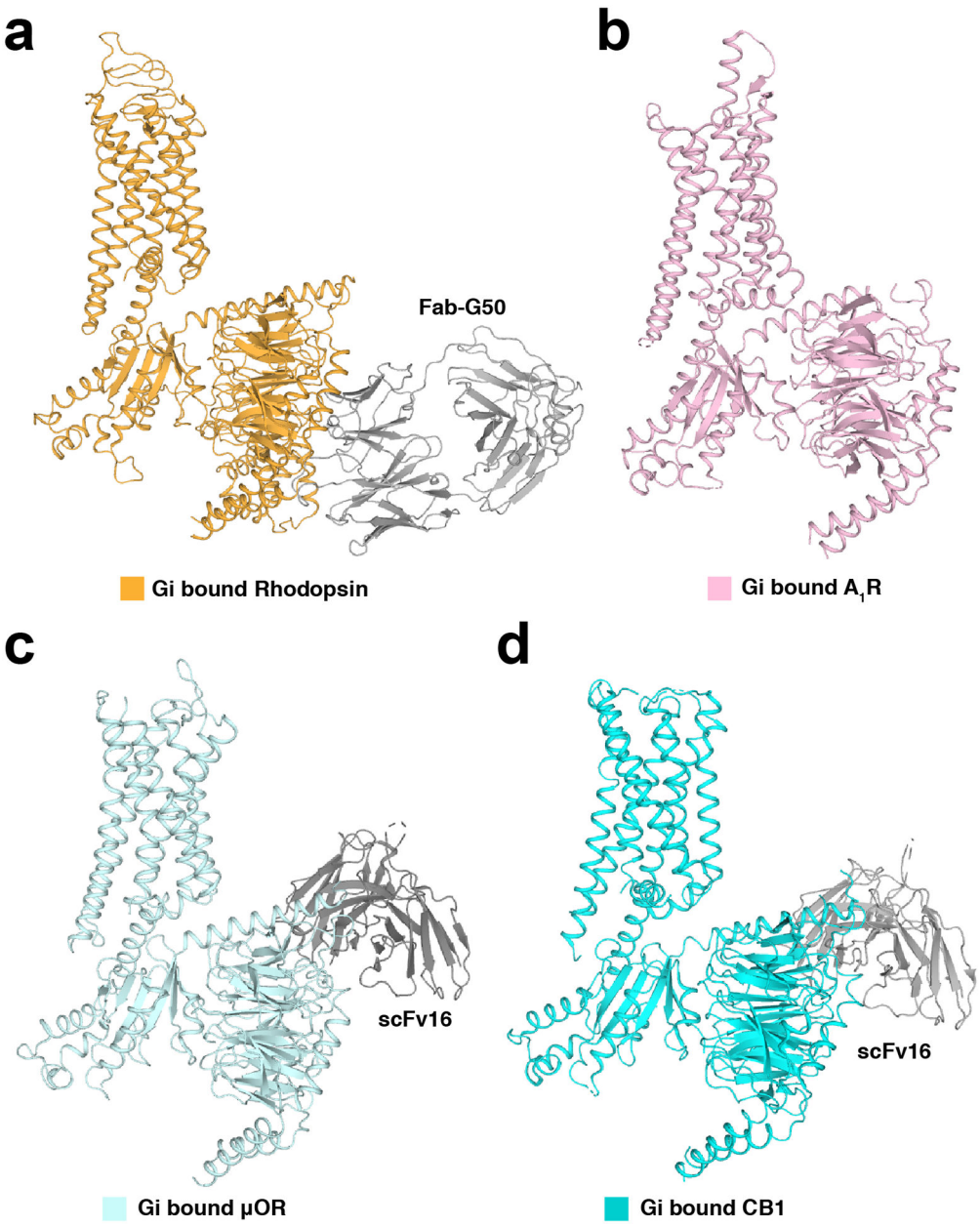

Extended Data Fig. 9. Comparison of the G_i coupled hSMO, inactive hSMO and apo hFZD4.
The G_i coupled hSMO is in blue, the inactive hSMO is in pink (PDB: 5L7D) and apo hFZD4 is in yellow (PDB: 6BD4). Structures are viewed from the side of the membrane.

Extended Data Table 1

Cryo-EM data collection, refinement and validation statistics

	hSMO–G_i–Fab complex (EMDB-20190) (PDB 6OTO)
Data collection and processing	
Magnification	46,729

	hSMO–G_i–Fab complex (EMDB-20190) (PDB 6OTO)
Voltage (kV)	300
Electron exposure (e−/Å^2)	70
Defocus range (μm)	−1.0 to −2.6
Pixel size (Å)	1.07
Symmetry imposed	C1
Initial particle images (no.)	469,244
Final particle images (no.)	141,100
Map resolution (Å)	3.84
FSC threshold 0.143	
Map resolution range (Å)	3.6–6.3
Refinement	
Initial model used (PDB code)	5L7D and 6CMO
Model resolution (Å)	4.4
FSC threshold 0.5	
Model resolution range (Å)	90–4.4
Map sharpening *B* factor (Å^2)	−100
Model composition	
Non-hydrogen atoms	10,572
Protein residues	1,345
Ligands	1
B factors (Å^2)	
Protein	205.58
Ligand	173.27
R.m.s. deviations	
Bond lengths (Å)	0.0081
Bond angles (°)	1.1594
Validation	
MolProbity score	1.53
Clashscore	3.20
Poor rotamers (%)	0.88
Ramachandran plot	
Favored (%)	93.62
Allowed (%)	6.38
Disallowed (%)	0.00

Acknowledgements

The data were collected at the UT Southwestern Medical Center Cryo-EM Facility (funded in part by the CPRIT Core Facility Support Award RP170644); we thank D. Stoddard for assistance in data collection. We thank E. Xu for sharing the materials for making Fab-G50; L. Beatty, A. Hassan and P. Schmiege for technical help; M. Brown, E. Debler, J. Goldstein, J. Jiang for discussion during manuscript preparation; B. Chen and J. Kim for $SMO^{-/-}$ MEFs. This work was supported by the Endowed Scholars Program in Medical Science of UT Southwestern Medical Center (to X.L.), O'Donnell Junior Faculty Funds (to X.L.), Welch Foundation (I-1957) (to X.L.), NIH grant P01 HL020948 (to J.M. and X.L.) and NIH grant 1R35GM128641 (to C.Z.). X.L. is a Damon Runyon-Rachleff Innovator supported by the Damon Runyon Cancer Research Foundation (DRR-53–19) and a Rita C. and William P. Clements, Jr. Scholar in Biomedical Research at UT Southwestern Medical Center.

References:

1. Jiang J & Hui CC Hedgehog signaling in development and cancer. Developmental cell 15, 801–812, doi:10.1016/j.devcel.2008.11.010 (2008). [PubMed: 19081070]
2. Petrov K, Wierbowski BM & Salic A Sending and Receiving Hedgehog Signals. Annual review of cell and developmental biology 33, 145–168, doi:10.1146/annurev-cellbio-100616-060847 (2017).
3. Arensdorf AM, Marada S & Ogden SK Smoothened Regulation: A Tale of Two Signals. Trends in pharmacological sciences 37, 62–72, doi:10.1016/j.tips.2015.09.001 (2016). [PubMed: 26432668]
4. Taipale J, Cooper MK, Maiti T & Beachy PA Patched acts catalytically to suppress the activity of Smoothened. Nature 418, 892–897, doi:10.1038/nature00989 (2002). [PubMed: 12192414]
5. Qi X, Schmiege P, Coutavas E, Wang J & Li X Structures of human Patched and its complex with native palmitoylated sonic hedgehog. Nature 560, 128–132, doi:10.1038/s41586-018-0308-7 (2018). [PubMed: 29995851]
6. Qi X, Schmiege P, Coutavas E & Li X Two Patched molecules engage distinct sites on Hedgehog yielding a signaling-competent complex. Science, doi:10.1126/science.aas8843 (2018).
7. Zhang Y et al. Structural Basis for Cholesterol Transport-like Activity of the Hedgehog Receptor Patched. Cell 175, 1352–1364 e1314, doi:10.1016/j.cell.2018.10.026 (2018). [PubMed: 30415841]
8. Pak E & Segal RA Hedgehog Signal Transduction: Key Players, Oncogenic Drivers, and Cancer Therapy. Developmental cell 38, 333–344, doi:10.1016/j.devcel.2016.07.026 (2016). [PubMed: 27554855]
9. Dunaeva M, Michelson P, Kogerman P & Toftgard R Characterization of the physical interaction of Gli proteins with SUFU proteins. The Journal of biological chemistry 278, 5116–5122, doi:10.1074/jbc.M209492200 (2003). [PubMed: 12426310]
10. Riobo NA, Saucy B, Dilizio C & Manning DR Activation of heterotrimeric G proteins by Smoothened. Proceedings of the National Academy of Sciences of the United States of America 103, 12607–12612, doi:10.1073/pnas.0600880103 (2006). [PubMed: 16885213]
11. Ogden SK et al. G protein Galphai functions immediately downstream of Smoothened in Hedgehog signalling. Nature 456, 967–970, doi:10.1038/nature07459 (2008). [PubMed: 18987629]
12. Byrne EFX et al. Structural basis of Smoothened regulation by its extracellular domains. Nature 535, 517–522, doi:10.1038/nature18934 (2016). [PubMed: 27437577]
13. Huang P et al. Cellular Cholesterol Directly Activates Smoothened in Hedgehog Signaling. Cell 166, 1176–1187 e1114, doi:10.1016/j.cell.2016.08.003 (2016). [PubMed: 27545348]
14. Huang P et al. Structural Basis of Smoothened Activation in Hedgehog Signaling. Cell 175, 295–297, doi:10.1016/j.cell.2018.09.003 (2018). [PubMed: 30241610]
15. Wang C et al. Structure of the human smoothened receptor bound to an antitumour agent. Nature 497, 338–343, doi:10.1038/nature12167 (2013). [PubMed: 23636324]
16. Wang C et al. Structural basis for Smoothened receptor modulation and chemoresistance to anticancer drugs. Nature communications 5, 4355, doi:10.1038/ncomms5355 (2014).
17. Huang HC & Klein PS The Frizzled family: receptors for multiple signal transduction pathways. Genome biology 5, 234, doi:10.1186/gb-2004-5-7-234 (2004). [PubMed: 15239825]
18. Sharpe HJ, Wang W, Hannoush RN & de Sauvage FJ Regulation of the oncoprotein Smoothened by small molecules. Nature chemical biology 11, 246–255, doi:10.1038/nchembio.1776 (2015). [PubMed: 25785427]
19. Raleigh DR et al. Cilia-Associated Oxysterols Activate Smoothened. Molecular cell 72, 316–327 e315, doi:10.1016/j.molcel.2018.08.034 (2018). [PubMed: 30340023]
20. Chen JK, Taipale J, Cooper MK & Beachy PA Inhibition of Hedgehog signaling by direct binding of cyclopamine to Smoothened. Genes & development 16, 2743–2748, doi:10.1101/gad.1025302 (2002). [PubMed: 12414725]
21. Nachtergaele S et al. Structure and function of the Smoothened extracellular domain in vertebrate Hedgehog signaling. eLife 2, e01340, doi:10.7554/eLife.01340 (2013). [PubMed: 24171105]
22. Kang Y et al. Cryo-EM structure of human rhodopsin bound to an inhibitory G protein. Nature 558, 553–558, doi:10.1038/s41586-018-0215-y (2018). [PubMed: 29899450]

23. Myers BR et al. Hedgehog pathway modulation by multiple lipid binding sites on the smoothened effector of signal response. Developmental cell 26, 346–357, doi:10.1016/j.devcel.2013.07.015 (2013). [PubMed: 23954590]
24. Weierstall U et al. Lipidic cubic phase injector facilitates membrane protein serial femtosecond crystallography. Nature communications 5, 3309, doi:10.1038/ncomms4309 (2014).
25. Draper-Joyce CJ et al. Structure of the adenosine-bound human adenosine A1 receptor-Gi complex. Nature 558, 559–563, doi:10.1038/s41586-018-0236-6 (2018). [PubMed: 29925945]
26. Garcia-Nafria J, Nehme R, Edwards PC & Tate CG Cryo-EM structure of the serotonin 5-HT1B receptor coupled to heterotrimeric Go. Nature 558, 620–623, doi:10.1038/s41586-018-0241-9 (2018). [PubMed: 29925951]
27. Koehl A et al. Structure of the micro-opioid receptor-Gi protein complex. Nature 558, 547–552, doi:10.1038/s41586-018-0219-7 (2018). [PubMed: 29899455]
28. Krishna Kumar K et al. Structure of a Signaling Cannabinoid Receptor 1-G Protein Complex. Cell 176, 448–458 e412, doi:10.1016/j.cell.2018.11.040 (2019). [PubMed: 30639101]
29. Wright SC et al. A conserved molecular switch in Class F receptors regulates receptor activation and pathway selection. Nature communications 10, 667, doi:10.1038/s41467-019-08630-2 (2019).
30. Huang W et al. Structural insights into micro-opioid receptor activation. Nature 524, 315–321, doi: 10.1038/nature14886 (2015). [PubMed: 26245379]
31. Yang S et al. Crystal structure of the Frizzled 4 receptor in a ligand-free state. Nature 560, 666–670, doi:10.1038/s41586-018-0447-x (2018). [PubMed: 30135577]
32. Corcoran RB & Scott MP Oxysterols stimulate Sonic hedgehog signal transduction and proliferation of medulloblastoma cells. Proceedings of the National Academy of Sciences of the United States of America 103, 8408–8413, doi:10.1073/pnas.0602852103 (2006). [PubMed: 16707575]
33. Chen W et al. Activity-dependent internalization of smoothened mediated by beta-arrestin 2 and GRK2. Science 306, 2257–2260, doi:10.1126/science.1104135 (2004). [PubMed: 15618519]
34. McDonald JG, Smith DD, Stiles AR & Russell DW A comprehensive method for extraction and quantitative analysis of sterols and secosteroids from human plasma. Journal of lipid research 53, 1399–1409, doi:10.1194/jlr.D022285 (2012). [PubMed: 22517925]
35. Rasmussen SG et al. Crystal structure of the beta2 adrenergic receptor-Gs protein complex. Nature 477, 549–555, doi:10.1038/nature10361 (2011). [PubMed: 21772288]
36. Zheng SQ et al. MotionCor2: anisotropic correction of beam-induced motion for improved cryo-electron microscopy. Nature methods 14, 331–332, doi:10.1038/nmeth.4193 (2017). [PubMed: 28250466]
37. Rohou A & Grigorieff N CTFFIND4: Fast and accurate defocus estimation from electron micrographs. Journal of structural biology 192, 216–221, doi:10.1016/j.jsb.2015.08.008 (2015). [PubMed: 26278980]
38. Scheres SH RELION: implementation of a Bayesian approach to cryo-EM structure determination. Journal of structural biology 180, 519–530, doi:10.1016/j.jsb.2012.09.006 (2012). [PubMed: 23000701]
39. Grigorieff N Frealign: An Exploratory Tool for Single-Particle Cryo-EM. Methods in enzymology 579, 191–226, doi:10.1016/bs.mie.2016.04.013 (2016). [PubMed: 27572728]
40. Emsley P & Cowtan K Coot: model-building tools for molecular graphics. Acta crystallographica. Section D, Biological crystallography 60, 2126–2132, doi:10.1107/S0907444904019158 (2004). [PubMed: 15572765]
41. Adams PD et al. PHENIX: a comprehensive Python-based system for macromolecular structure solution. Acta crystallographica. Section D, Biological crystallography 66, 213–221, doi:10.1107/S0907444909052925 (2010). [PubMed: 20124702]
42. Murshudov GN, Vagin AA & Dodson EJ Refinement of macromolecular structures by the maximum-likelihood method. Acta crystallographica. Section D, Biological crystallography 53, 240–255, doi:10.1107/S0907444996012255 (1997). [PubMed: 15299926]
43. Brown A et al. Tools for macromolecular model building and refinement into electron cryo-microscopy reconstructions. Acta crystallographica. Section D, Biological crystallography 71, 136–153, doi:10.1107/S1399004714021683 (2015). [PubMed: 25615868]

44. Eyck LFT Efficient structure-factor calculation for large molecules by the fast fourier transform. Acta Crystallogr. A 33, 486–492 (1977).

45. Wang Z et al. An atomic model of brome mosaic virus using direct electron detection and real-space optimization. Nature communications 5, 4808, doi:10.1038/ncomms5808 (2014).

46. Heymann JB & Belnap DM Bsoft: image processing and molecular modeling for electron microscopy. Journal of structural biology 157, 3–18, doi:10.1016/j.jsb.2006.06.006 (2007). [PubMed: 17011211]

47. Chen VB et al. MolProbity: all-atom structure validation for macromolecular crystallography. Acta crystallographica. Section D, Biological crystallography 66, 12–21, doi:10.1107/S0907444909042073 (2010). [PubMed: 20057044]

48. Pettersen EF et al. UCSF Chimera--a visualization system for exploratory research and analysis. Journal of computational chemistry 25, 1605–1612, doi:10.1002/jcc.20084 (2004). [PubMed: 15264254]

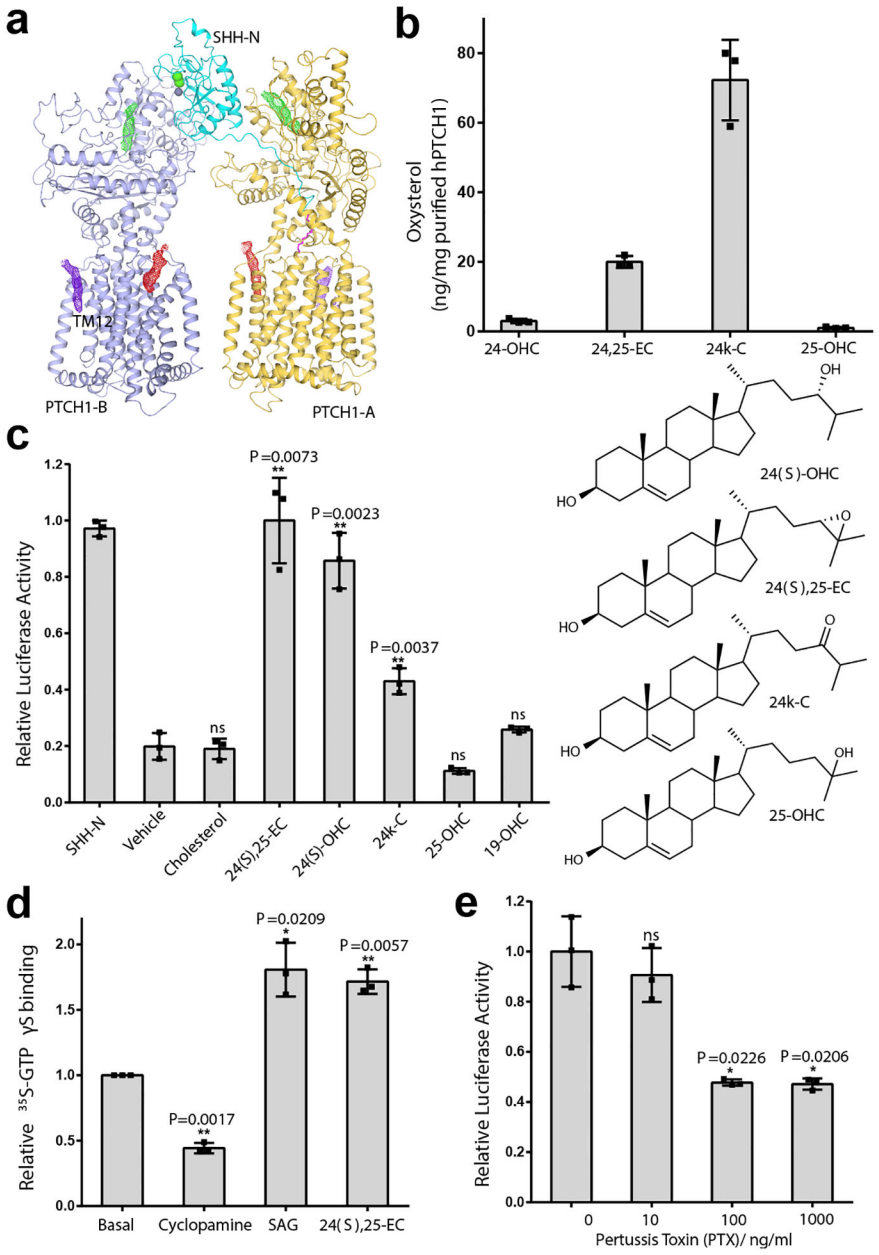

Fig. 1. Functional characterization of PTCH1-associated oxysterols in HH signaling.

a, The sterol-like densities in the SHH-N mediated PTCH1 dimer. Sterol-like densities at 5s level at 3.5 Å resolution in the domains of ECD-I, SSDs and near TM-12 are colored in green, red and purple, respectively. **b**, HPLC-MS quantitation of oxysterols extracted from purified PTCH1 protein. Data are mean ± s.d. (n = 3 biologically independent experiments). Oxysterol structures are shown. **c**, Oxysterol-mediated HH signaling. The SHH-light II cells were treated with vehicle (0.3 mM MCD), MCD complexed with 30μM sterol or SHH-N conditioned media. **d**, GTPγS binding assay. Basal represents the hSMO basal activity without ligand. All ligands were used at a saturating concentration of 50 μM. **e**, PTX decreases the 24(*S*),25-EC mediated HH signaling. HH activity was measured by dual-luciferase assay. Each assay in **c-e** was repeated at least three times with similar results and

data are mean ± s.d. (n = 3 biologically independent experiments). *$P \leq 0.05$, **$P \leq 0.01$, two-sided t-test using GraphPad Prism 7.

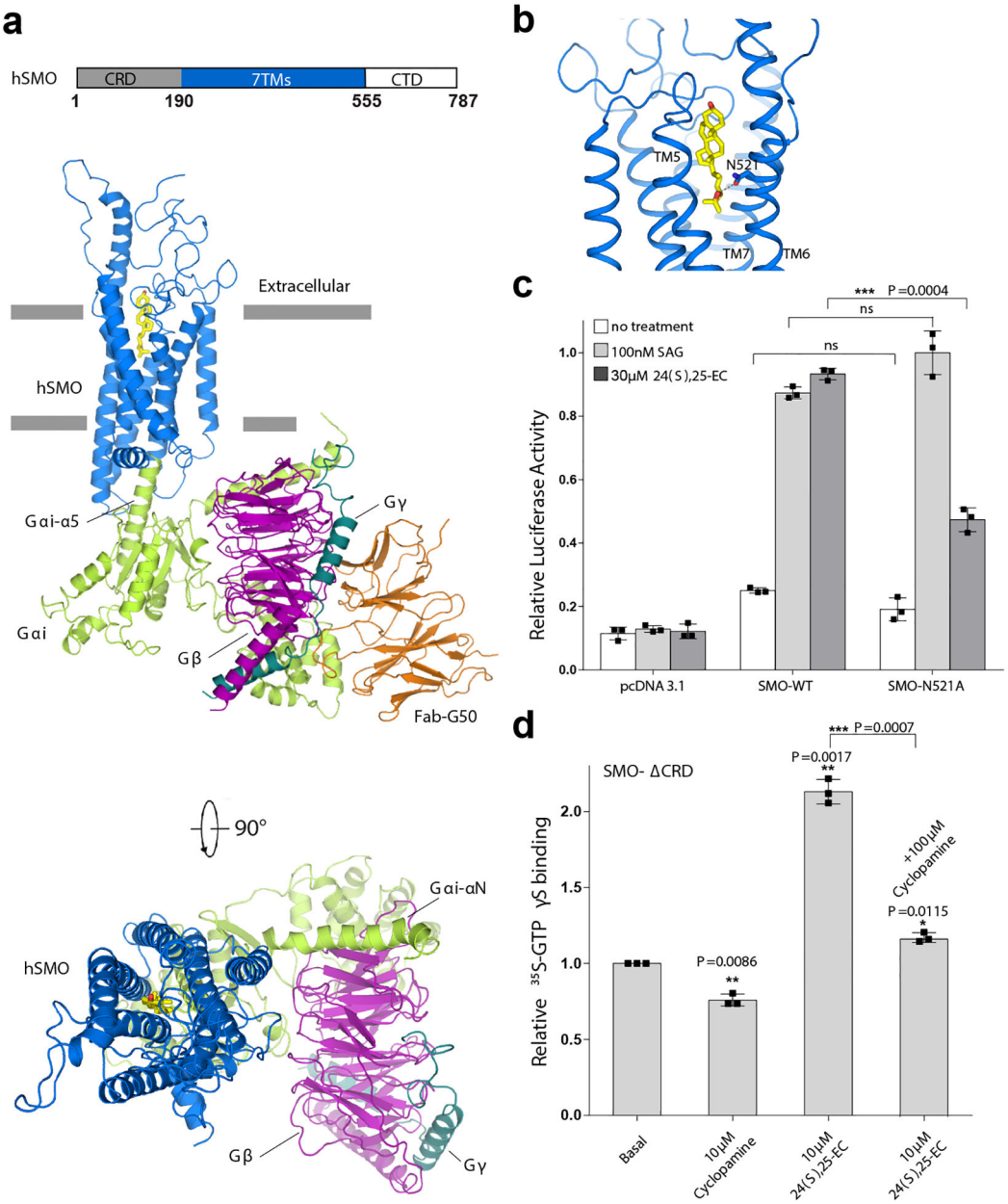

Fig. 2. Structure of hSMO–G_i–Fab complex.

a, Ribbon representation of the complex structure. Primary structure of hSMO is on the top. Residues 556–787 of hSMO were removed for protein expression and the CRD domain (gray) was not determined in the cryo-EM map. hSMO, Gα, Gβ, Gγ and Fab-G50 are colored in blue, green, magenta, dark teal and orange; the putative 24(*S*),25-EC is shown as yellow sticks. **b**, The ligand-binding pocket. The putative ligand and its bound residue are shown as sticks. **c**, HH signaling in *Smo*$^{-/-}$ MEFs transfected with pcDNA3.1, full-length hSMO-wild type (WT) or full-length hSMO-N521A mutant and response to SAG or 24(*S*), 25-EC via luciferase activity. **d**, The GTPγS binding competition assay using cells overexpressing hSMO-ΔCRD. The assays were set up as Fig. 1d with various ligand concentrations. Each assay in **c-d** was repeated at least three times with similar results and

data are mean ± s.d. (n = 3 biologically independent experiments). *$P \leq 0.05$, **$P \leq 0.01$, ***$P \leq 0.001$, two-sided t-test using GraphPad Prism 7.

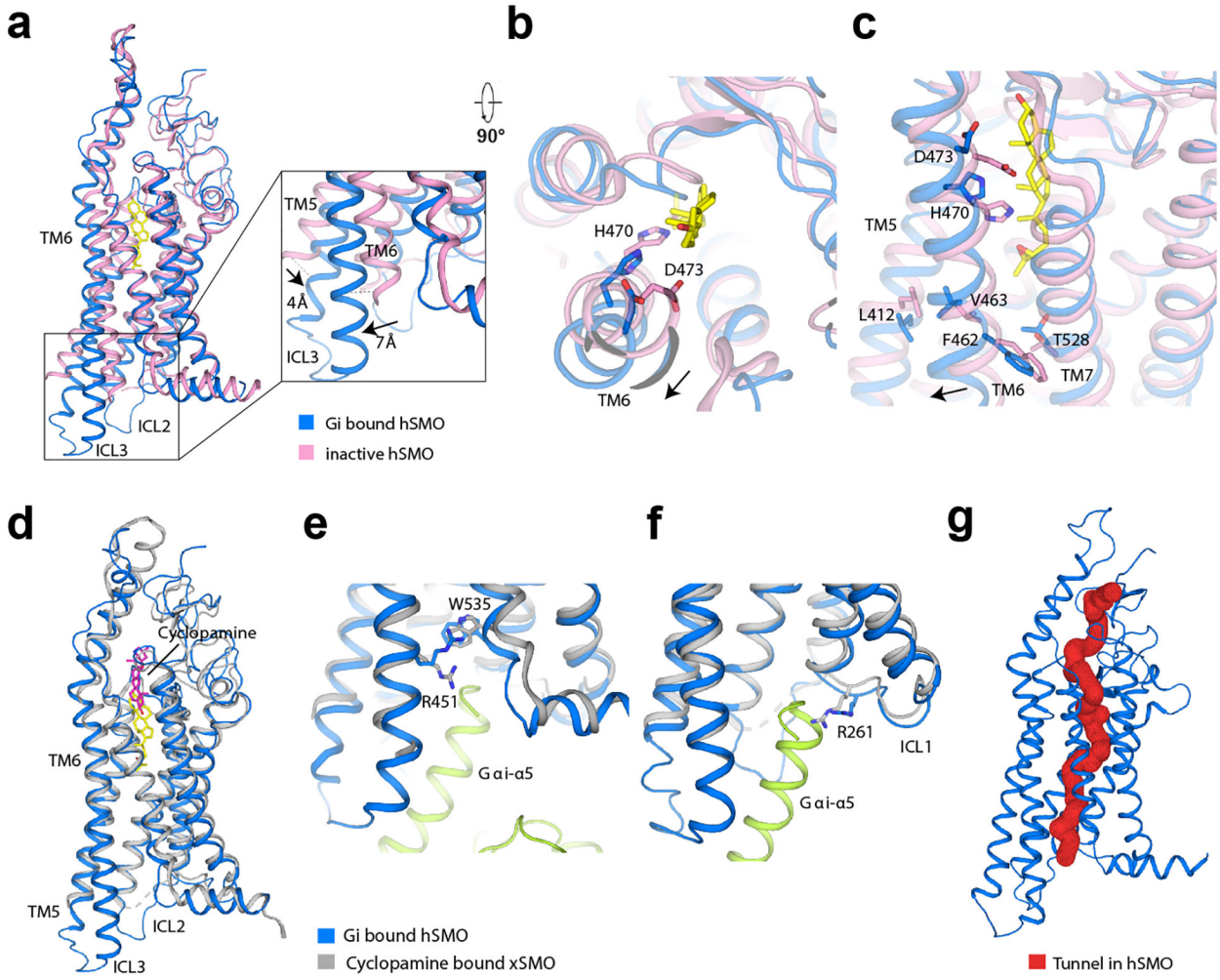

Fig. 3. Structural comparison of the G_i-bound hSMO with inactive hSMO and cyclopamine bound xSMO.

a, Superimposition of TMs of hSMO molecules. G_i-coupled hSMO is colored in blue, inactive hSMO (PDB: 5L7D) is colored in pink. The movements of structural elements are indicated. **b**, Movement of TM6 in the G_i-coupled hSMO due to ligand binding. **c**, Movements of TMs 5–7 in the G_i-coupled hSMO compared with the inactive hSMO. The related residues are shown as sticks. **d**, Superimposition of 7-TMs of hSMO (blue) and xSMO (PDB: 6D32, gray). **e**, Comparison of R451 and W535 in G_i-coupled hSMO with the corresponding residues in xSMO. **f**, Comparison of the ICL1 of hSMO and xSMO. R261 and its corresponding residue in xSMO are shown. **g**, The putative tunnel in hSMO is shown as red mesh.

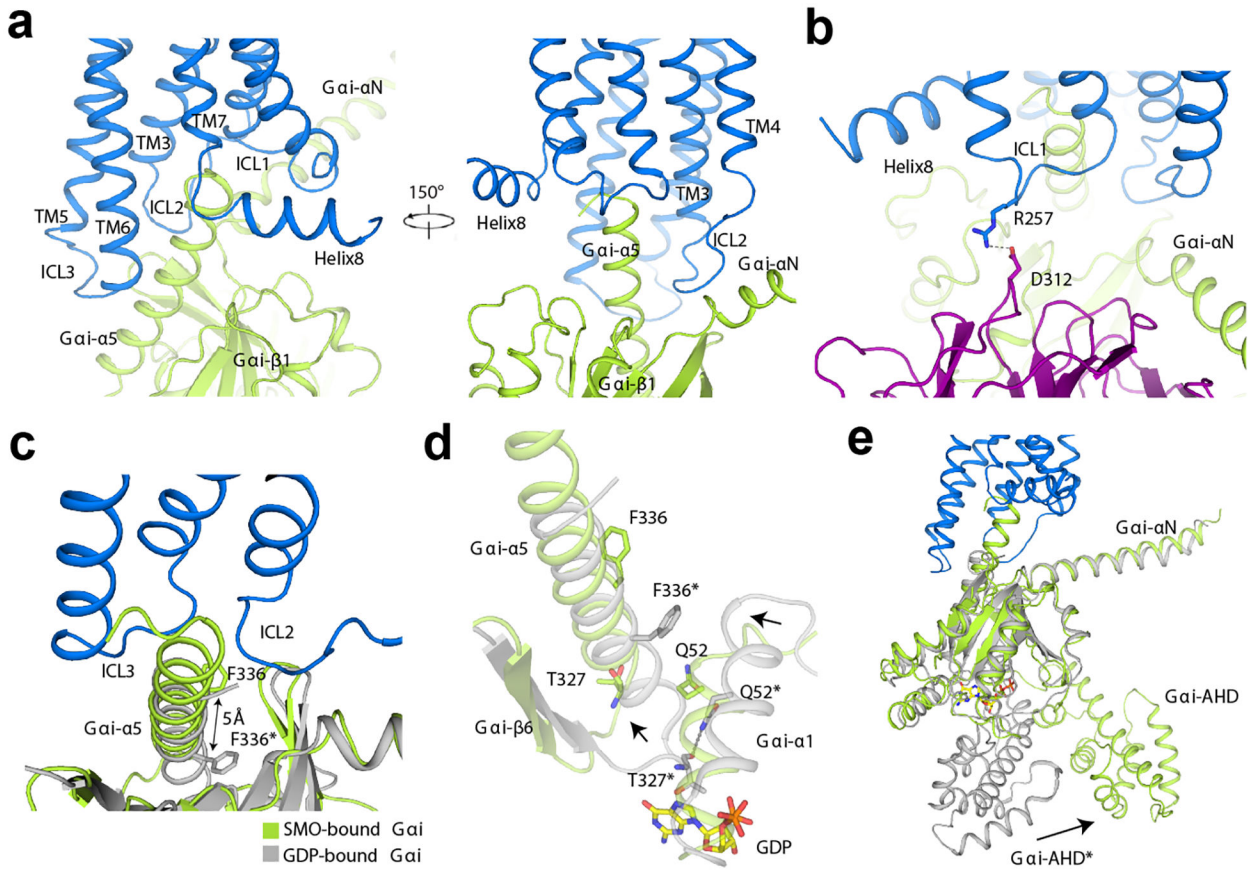

Fig. 4. Conformational changes in G_i upon coupling to hSMO.

a, The interaction details between hSMO (blue) and $G\alpha_i$ (green). The structural elements involved in the interaction are indicated. **b**, R257 in hSMO-ICL1 binds D312 of Gβ. Both residues are labeled and shown. **c** and **d**, Comparison of GDP-bound $G\alpha_i$ (PDB: 1GP2, gray) and nucleotide-free $G\alpha_i$ (green) from hSMO–G_i complex. GDP is shown as yellow sticks. **e**, Structural rearrangement of $G\alpha_i$-AHD domain after coupling to hSMO.

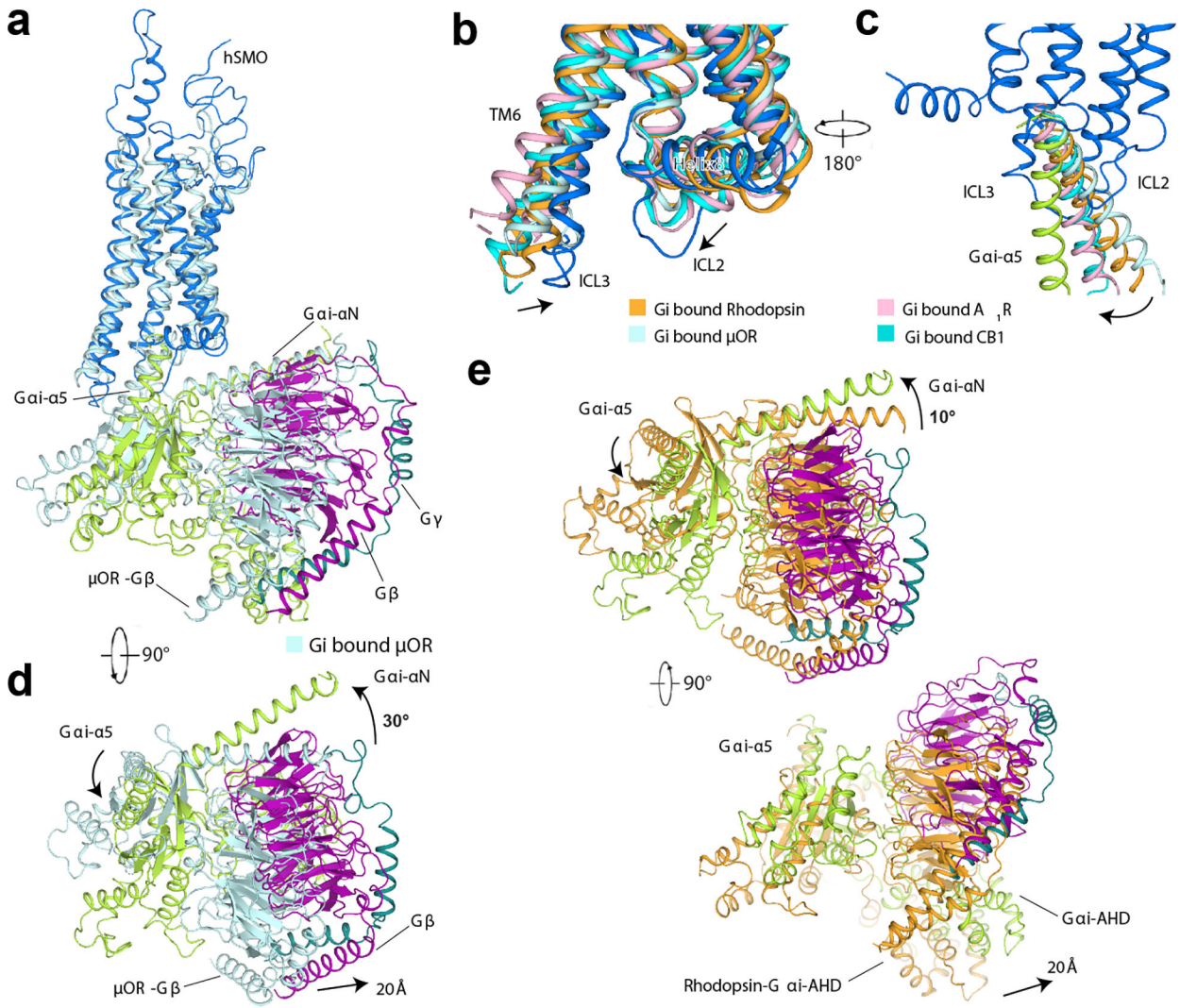

Fig. 5. Distinct orientations of heterotrimeric G_i proteins after coupling to hSMO and Class-A GPCRs.

a, Structural comparison of hSMO-G_i complex with μOR-G_i complex (PDB: 6DDE, light cyan). The $G\alpha_i$-α5 and $G\alpha_i$-αN are indicated. hSMO, Gα, Gβ and Gγ in hSMO-G_i complex are colored as Fig. 2a. **b**, The comparison of the ICL2 and ICL3 among the five GPCR-G_i complexes. The structural elements from Rhodopsin-G_i (PDB: 6CMO) are in orange; from A_1R-G_i (PDB: 6D9H) are in pink, from μOR-G_i are in light cyan and from CB1-G_i (PDB: 6N4B) are in cyan. **c**, The comparison of the $G\alpha_i$-α5 among the five GPCR-G_i complexes. **d**, The structural comparison of G_i proteins after coupling μOR and hSMO. **e**, The structural comparison of G_i proteins after coupling rhodopsin and hSMO. The major differences of G_i protein orientations are indicated.